

Text2Control3D: Controllable 3D Avatar Generation in Neural Radiance Fields using Geometry-Guided Text-to-Image Diffusion Model

Sungwon Hwang, Junha Hyung, Jaegul Choo

Graduate School of Artificial Intelligence, KAIST
 {shwang.14, sharpeee, jchoo}@kaist.ac.kr

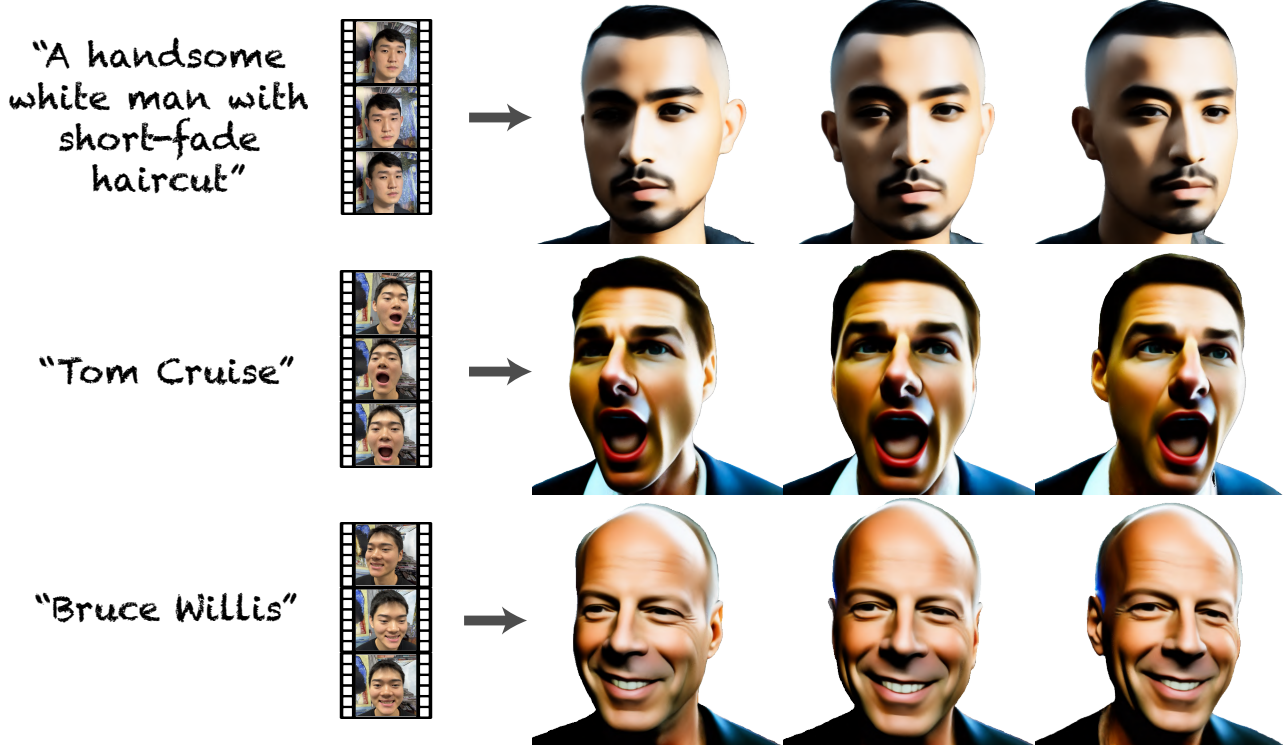


Figure 1: **Text2Control3D** can generate a 3D avatar given a text description and a casually captured monocular video for conditional control of facial expression and shape.

Abstract

Recent advances in diffusion models such as ControlNet have enabled geometrically controllable, high-fidelity text-to-image generation. However, none of them addresses the question of adding such controllability to text-to-3D generation. In response, we propose Text2Control3D, a controllable text-to-3D avatar generation method whose facial expression is controllable given a monocular video casually captured with hand-held camera. Our main strategy is to construct the 3D avatar in Neural Radiance Fields (NeRF) optimized with a set of controlled viewpoint-aware images that we generate from ControlNet, whose condition input is the depth map extracted from the input video. When generating the viewpoint-aware images, we utilize cross-reference attention to inject well-controlled, referential facial expression and appearance via cross attention. We also conduct low-pass filtering of Gaussian latent of the diffusion model in order to ameliorate the viewpoint-agnostic texture problem we observed from our empirical analysis, where the viewpoint-aware images contain identical textures on identical pixel positions that are in-

comprehensible in 3D. Finally, to train NeRF with the images that are viewpoint-aware yet are not strictly consistent in geometry, our approach considers per-image geometric variation as a view of deformation from a shared 3D canonical space. Consequently, we construct the 3D avatar in a canonical space of deformable NeRF by learning a set of per-image deformation via deformation field table. We demonstrate the empirical results and discuss the effectiveness of our method.

Introduction

Recently, large text-to-image diffusion models (Ramesh et al. 2022; Saharia et al. 2022; Rombach et al. 2021) have enabled visually-appealing image generation that faithfully reflects the semantics of conditional texts. Such works have greatly impacted the generative models to be widely used for non-expert users, as the models can generate high-quality images of interest using text descriptions only. Moreover, ControlNet (Zhang and Agrawala 2023) further extended

the utility of the models by proposing the method to add geometric control such as canny edge, human pose, depth map, and normal map for geometrically controlled text-conditional image generation.

Meanwhile, Text-to-3D generation methods such as DreamFusion (Poole et al. 2022) have been proposed using Neural Radiance Fields (Mildenhall et al. 2020) as a 3D representation, and proved to yield promising quality of generation. However, no work has tackled the question of adding geometric controllability to text-to-3D generation, despite its importance highlighted by ControlNet and its impact to the research community.

Parallel to ControlNet extracting geometric control factors from a source image for generative conditions, we propose a method to generate text-conditional 3D facial avatars conditioned with geometric control factors extracted from a casually-captured monocular video of a face. As a pioneering work, we focus on controllability in terms of the facial expressions and shapes for 3D avatar generation, which are the key functionalities of an avatar to behave as a faithful, virtual agent. Specifically, given a text description and a casually-captured monocular video for conditional control, our method generates a 3D avatar that reflects the semantics of the text as well as facial expression and deformation of the source face as in Fig. 1.

Our main strategy comprises the following procedures. First, we generate a set of viewpoint-aware images of an avatar, whose facial expressions and shapes are controlled using geometry-conditional text-to-image diffusion model such as ControlNet. Then, the generated images are used to construct the avatar in NeRF. In doing so, we define three problems raised and solved by our method, which as a whole yields the state-of-the-art 3D avatar generation quality and controllability compared to existing works.

When leveraging ControlNet to generate viewpoint-aware images, injecting constant appearance and desired facial expression across the images is one key objective for well-controlled avatar generation. To do so, we propose cross-reference attention, a zero-shot method for the diffusion model where viewpoint-aware image generations conduct a cross-attention to a shared, referential information of controlled facial expression and appearance.

Another objective is to ameliorate the texture-sticking problem, the phenomena where images generated with slight spatial variations of latent contain constant, spatial variation-agnostic textures (Karras et al. 2021). We observed that our viewpoint-aware images conditioned with slightly varying geometric conditions also suffer from similar problem. Such disrupts high-quality 3D avatar construction, as sticking textures are not geometrically interpretable and becomes the key factor of unwanted artifacts. In this work, we show that the sticking textures are originated from high-frequency components of the Gaussian latent. From the observation, we propose a method to remove the sticking textures by filtering high-frequency components of the Gaussian latent in Fourier domain, and re-injecting texture-sticking-free details via cross-attention to full-frequency features.

The final objective of our method is to construct 3D avatar given the viewpoint-aware images that are not strictly con-

sistent in geometry. Our insight is to interpret such inconsistencies as views of per-image deformations from a canonical 3D model. Inspired by recent advancements in deformable NeRFs (Park et al. 2021a,b), we train deformation field table, a set of per-image 3D deformation code, and construct a shared, 3D canonical model as our final 3D avatar.

In summary, our work makes four major contributions:

- From the best of our knowledge, Text2Control3D is the first controllable Text-to-3D avatar generation method.
- We propose a zero-shot method of ControlNet that generates a set of viewpoint-aware avatar images with constant appearance and controlled facial expression.
- We observe and ameliorate the texture-sticking problem in viewpoint-aware images generated from ControlNet.
- We propose a method to reconstruct high-fidelity 3D avatar given a set of generated viewpoint-aware images.

Related Works

Neural Radiance Fields First proposed by (Mildenhall et al. 2020), Neural Radiance Field (NeRF) is an implicit representation of 3D space, which is an MLP that predicts a color and density of 3D points. These are then rendered with volume rendering techniques and supervised with dense set of posed images for optimization. Following works include dynamic scene reconstruction with deformable NeRF (Pumarola et al. 2021; Park et al. 2021a,b), or latent-conditional NeRF for generative 3D models using GANs (Chan et al. 2021, 2022; An et al. 2023).

Text-to-2D/3D Diffusion Models Recent advancements in text-to-image diffusion models such as DALL-E (Ramesh et al. 2021), Imagen (Saharia et al. 2022), and Latent Diffusion Models (Rombach et al. 2021) have brought great advancements in text-driven high-fidelity image generations. Following works such as GLIGEN (Li et al. 2023) or ControlNet (Zhang and Agrawala 2023) propose a method to generate images that satisfy geometric conditions such as depth, normal, or key-point maps.

Meanwhile, a line of work in 3D generation leverages distillation from large-scale text-to-image diffusion model to 3D via per-text optimization in NeRF. Notably, Score Distillation Sampling (Poole et al. 2022) and their variants (Lin et al. 2023; Chen et al. 2023) approximate the gradients of parameters of 3D representations with reverse diffusion guidance of large-scale text-to-image diffusion model. Other methods include image-to-3D generation (Liu et al. 2023a,b; Anciukevičius et al. 2023), which can conduct text-to-3D generation given a text-to-image diffusion model, or diffusion models in 3D space (Shue et al. 2023; Luo and Hu 2021), which require 3D assets for training data.

Proposed Method

In this section, we propose a pipeline to generate a 3D face avatar given a text description c_{text} , (e.g. *"Elon Musk"*, *"A handsome white man with short-fade haircut"*), and frames of a monocular video $\mathcal{I} = \{I_1 \dots I_L\}$ for facial expression and shape control.

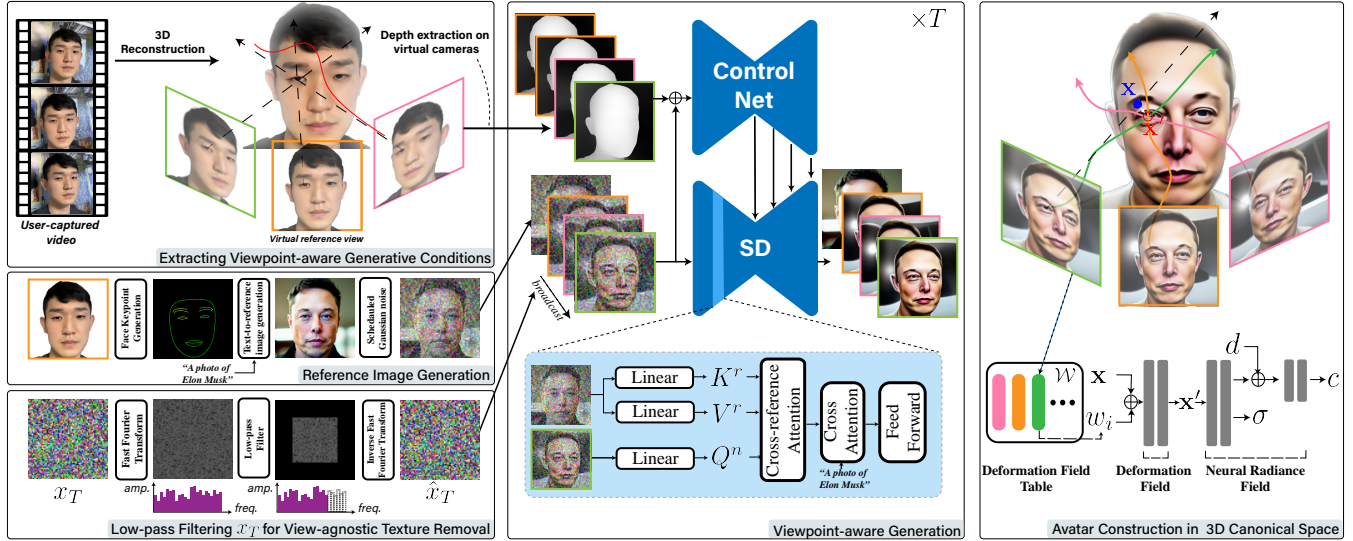


Figure 2: Illustration of Text2Control3D, our controllable text-to-3D avatar generation method.

To do so, we first extract viewpoint-augmented depth maps from a monocular video. Then, we use these depth maps as conditions for generating viewpoint-aware avatar images using ControlNet enhanced with (1) cross-reference attention to achieve controllability on facial expression and appearance across the viewpoint-aware generations, and (2) low-pass filtering of Gaussian latent to remove view-agnostic textures that break 3D consistency. Finally, we regard remaining inconsistencies in geometry as views of per-image deformation of 3D canonical space. As so, we train deformation field table that encodes per-view deformation code to finally construct the 3D avatar in NeRF canonical space. The summary is illustrated in Fig. 2.

Viewpoint-aware Generative Conditions

First, we create a set of generative conditions from monocular video frames. We use depth maps for these conditions, as we empirically learned that they contain sufficient viewpoint knowledge while preserving reasonable amount of source geometry information that do not collide with semantics of text conditions. Instead of retrieving depth maps from input video frames, we use these frames to reconstruct the scene, followed by rendering depth maps from virtual cameras as means of augmenting to denser depth map construction.

Specifically, we first reconstruct the source face into 3D in NeRF (Mildenhall et al. 2020) using the input monocular video frames. That is, we find

$$\theta_{src}^* = \underset{\theta_{src}}{\operatorname{argmin}} \sum_{l=1}^L \|I_l - g(\theta_{src}; T_l^{src})\|_2, \quad (1)$$

via gradient-descent optimization, where θ_{src} is the parameter of NeRF MLP, $g(\cdot)$ is a volume rendering function (Mildenhall et al. 2020), $T_l^{src} \in \mathcal{T}^{src}$ is a camera parameter of a frame I_l .

Using θ_{src}^* , we then render depth maps $\mathcal{D} = \{D_1 \dots D_N\}$ on a set of augmented virtual cameras $\mathcal{T} = \{T_1 \dots T_N\}$ as

$$D_n = g_d(\theta_{src}^*; T_n), \quad (2)$$

where $D_n \in \mathcal{D}$, $T_n \in \mathcal{T}$, and g_d is a volumetric depth rendering function, or a monocular depth estimation on correspondingly rendered images.

Viewpoint-aware Image Generation

Given our viewpoint-aware generative conditions \mathcal{D} and c_{text} , a vanilla method to generate viewpoint-aware images of an avatar $\mathcal{X} = \{x^1 \dots x^N\}$ using depth-conditional ControlNet G_d would be

$$x^n = G_d(D_n, c_{text}, x_T^n), \quad (3)$$

where $x_T \sim \mathcal{N}(0, 1)$ and $x_T \rightarrow x_T^n$ for all n . However, we make empirical analysis of Eq. (3) and learned that it yields sub-optimal quality for viewpoint-aware generation. As so, we propose two methods, cross-reference attention and low-pass filtering of Gaussian latent, which are zero-shot methods to ControlNet.

Cross-reference Attention We empirically learned and reported following qualitative results in the first column of Fig. 6-(a) that per-frame avatar image generation using Eq. (3) has two undesirable properties for viewpoint-aware avatar image generation. First, depth condition alone cannot reliably convey detailed facial expressions. Second, generated images conditioned with depth images of far-distanted virtual cameras vary in their visual appearances, even though they are generated from the same Gaussian latent.

As so, we propose cross-reference attention, a method that induces reverse diffusion processes to attend to a shared information of controlled facial expression and appearance. Specifically, we first extract a desired face key-point from the image of the source rendered at a virtual reference view. Then, we generate a reference image \bar{x}^r using the face key-point, c_{text} and another key-point conditional ControlNet G_{kp} . Formally,

$$k^r = K(g(\theta_{src}^*; T^r)) \quad (4)$$

$$\bar{x}^r = G_{kp}(k^r, c_{text}), \quad (5)$$

where $T^r \in \mathcal{T}$ is a virtual reference camera, and $K(\cdot)$ is a face key-point estimator.

Then, we devise the feature maps in our viewpoint-aware generator G_d to attend to the reference image via cross attention as

$$Q^n = MLP_Q(h_t^n), \quad (6)$$

$$K^r, V^r = MLP_{K,V}(\bar{h}_t^r), \quad (7)$$

where h_t^n is the feature map of x_t^n , and \bar{h}_t^r is the feature map of $\bar{x}_t^r \sim \mathcal{N}(\sqrt{\bar{\alpha}_t} \bar{x}_r, (1 - \bar{\alpha}_t) \mathbf{I})$, the reference image noised with scheduled step of t (Ho, Jain, and Abbeel 2020). Effectively, we may replace the self-attention modules to our cross-reference attention.

$$\text{Attention}(Q^n, K^r, V^r) = \text{softmax}\left(\frac{Q^n(K^r)^\top}{\sqrt{c}}\right)V^r. \quad (8)$$

View-agnostic Texture Removal We empirically found that the generated images suffer from the texture-sticking problem (Karras et al. 2021), the phenomena that the images share constant textures in image space despite of spatial variations in generative conditions, which we dub as view-agnostic texture in our work. Specifically, we generated avatar images using vanilla ControlNet conditioned with depth maps rendered from 13 adjacent virtual cameras, and averaged the images. Left side and right-side of Fig. 3-(a) are the averaged image and the image generated with the depth map rendered from a virtual camera located at the center of the 13 cameras. As can be seen, some textural details of the two images are identical, which is possible only when the textures of the most generated images are located at an identical position in image space. These eventually create undesirable artifacts when used to construct 3D avatars in later sections. As so, we propose a method to remove such view-agnostic textures while preserving most high-fidelity details, as seen in Fig. 3-(b).

We learned that high-frequency components in the Gaussian latent x_T is the key factor that generates such textures. As so, we first remove the high-frequency components of the Gaussian latent in Fourier domain as

$$\hat{x}_T^n = f^{-1}(P(f(x_T^n), b)), \quad (9)$$

where f and f^{-1} are Fast Fourier Transform and Inverse Fast Fourier transform (Brigham 1988), respectively, P is a low-pass filter that removes the frequency components higher than b , a cut-off frequency.

Then, high-fidelity details are re-injected via cross-attention to full-frequency features as

$$Q^n = MLP_q(\hat{h}_t^n), \quad (10)$$

$$K^n, V^n = MLP_{K,V}(h_t^n), \quad (11)$$



Figure 3: (a) Empirical analysis of the texture-sticking problem observed from images generated with ControlNet conditioned with depth rendered from adjacent cameras. (b) Our method ameliorates the problem by removing the sticking textures while preserving most high-fidelity details.

where \hat{h}_t^n is the feature map of \hat{x}_T^n . In this case, h_t^n is the feature map of x_t^n that goes through an independent reverse diffusion process from x_T in parallel. Design choice of cross-attention to full-frequency features instead of self-attention will be discussed in ablation study.

Finally, we merge both cross-reference attention and view-agnostic texture removal into a single attention pipeline by replacing h_t^n in Eq. (11) with \bar{h}_t^r as

$$Q^n = MLP_q(\hat{h}_t^n), \quad (12)$$

$$K^r, V^r = MLP_{K,V}(\bar{h}_t^r). \quad (13)$$

Formally, Eq. (3) is reformulated to define our final viewpoint-aware image generator as

$$x^n = G_d^*(D_n, D_r, c_{text}, \hat{x}_T^n, \bar{x}^r), \quad (14)$$

where G_d^* replaces self-attention with our cross-reference attention that comprises Eq. (12), Eq. (13), and Eq. (8), and D_r is depth map rendered from a virtual reference camera using θ_{src}^* , which is used as a depth condition for calculating \bar{h}_t^r . In addition, cross-reference attention is conducted on time-steps larger than t_{thres} to regularize facial expression and appearances on earlier stages, whereas self-attention replaces the cross-reference attention on later stages to concentrate on viewpoint-specific generations.

3D Avatar Construction in Canonical Space

Using \mathcal{X} , a set of generated viewpoint-aware avatar images, we now reconstruct a 3D avatar model in NeRF. Since the generated images are not strictly consistent in geometry, direct reconstruction may yield broken results and unwanted artifacts. Instead, we assume that all images share a single 3D canonical model, and regard per-image geometric inconsistency as a view of a deformed canonical model.

Specifically, we first define learnable deformation field table, $\mathcal{W} = \{w_1 \dots w_N\}$, where $w_n \in \mathcal{W}$ is assigned to each virtual view. Then, we define a canonical 3D model parameter $\Theta = \{\theta_d, \theta_c\}$, where each deformation code w_n learns to project a point in observation space \mathbf{x} to the shared canonical space, after which a shared MLP predicts the view-direction dependent color and density of the point as

$$\mathbf{x}' = F(\mathbf{x}; \theta_d, w_n), \quad (15)$$

$$(c, \sigma) = F'(\mathbf{x}', d; \theta_c), \quad (16)$$



Figure 4: Visualization of 3D avatars generated with our method.

where F and F' are MLP forward functions, and d is a view direction in observation space. We optimize Θ and \mathcal{W} to minimize the difference between the generated avatar images \mathcal{X} and images rendered from our deformed canonical space. Also, we do not reconstruct backgrounds in generated images, as they are not viewpoint-aware and are irrelevant to avatar reconstruction. As so, we use off-the-shelf face segmentation network to generate a set of per-image mask $M_n \in \mathcal{M} = \{M_1 \dots M_N\}$, and apply sparsity loss, which encourages the point samples of camera rays projected to background region to yield low density, thus emptying the corresponding space.

Also, we learned that the canonical NeRF occasionally converges to semi-transparent object density in order to explain the geometric inconsistencies between viewpoint-aware images. As so, we apply entropy loss (Kim, Seo, and Han 2022), which maximizes the Shannon entropy (Shannon 1948) of the density distribution of a ray pro-

jected to foreground. Such prior encourages the object to maximize the density closer to the object surface and to suppress the density farther from the object surface, thus discouraging semi-transparent surfaces of 3D canonical avatar. In summary, we minimize the following loss for 3D avatar reconstruction, $\mathcal{L}_{NeRF} = \lambda_{RGB}\mathcal{L}_{RGB} + \lambda_{sp}\mathcal{L}_{sp} + \lambda_{entropy}\mathcal{L}_{entropy}$, where

$$\mathcal{L}_{RGB} = \sum_n \|M_n \otimes (x^n - g(\Theta, w_n; T_n))\|_2, \quad (17)$$

$$\mathcal{L}_{sp} = \frac{1}{J} \sum_{n,j,h,w} |1 - \exp(-\lambda\sigma_j)| \cdot (1 - m_n^{(h,w)}), \quad (18)$$

$$\mathcal{L}_{entropy} = - \sum_{n,j,h,w} p(\alpha_j) \log p(\alpha_j) \cdot m_n^{(h,w)}, \quad (19)$$

where $m_n^{(h,w)}$ is a binary value of M_n located at (h, w) pixel location, $\{\sigma_j\}_{j=1}^J$ are density values evaluated from points

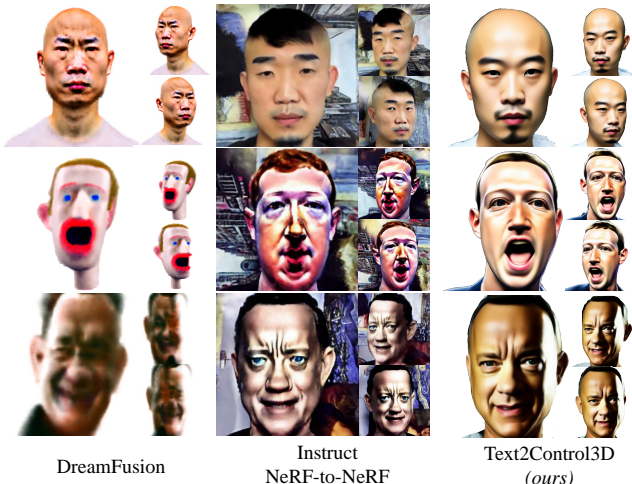


Figure 5: Qualitative comparisons to baselines. Text conditions are “A bald Asian man with goatee”, “Mark Zuckerberg”, and “Tom Hanks” for each row from the top.

sampled from the ray propagating from (h, w) of image plane located at T_n , $p(\alpha_j) = \frac{\alpha_j}{\sum_{i=1}^J \alpha_i} = \frac{1 - \exp(-\sigma_j \delta_j)}{\sum_{i=1}^J 1 - \exp(-\sigma_i \delta_i)}$ is the normalized point opacity, and λ_{RGB} , λ_{sp} , $\lambda_{entropy}$ are hyper-parameters.

Experiments

Dataset Volunteers were instructed to make three distinct and extreme facial expressions: neutral face, smiling, and opened mouth, in order to validate the range of expressibility. For text conditions, we created two sets of text prompts, each containing 23 number of texts: one is a set of names of celebrities, and the other is a set of descriptions of facial attributes.

Implementation Details We generate view-point aware images in 512×512 resolution. ControlNet conducts reverse diffusion process in latent space defined by pre-trained auto-encoder (Rombach et al. 2021), making spatial dimension of Fourier spectrum to be 64×64 , which is the latent space resolution. We use $b = 22$ for attribute description texts, and $b = 18$ for celebrity name texts for low-pass filtering in Fourier space. Algorithmically, low-pass filter P replaces the values in Fourier spectrum outside the $(2 \cdot b) \times (2 \cdot b)$ box located at the spectrum center with 0. For reverse diffusion process of ControlNet, we used DDIM (Song, Meng, and Ermon 2020) with 50 steps, and $t_{thres} = 45$ for cross-reference attention. For canonical 3D avatar reconstruction, we used $\lambda_{RGB} = 1$, $\lambda_{sp} = 1 \times 10^{-3}$, and $\lambda_{sp} = 1 \times 10^{-6}$.

Baselines Since no work tackles the controllable text-to-3D generation from the best of our knowledge, we make qualitative comparisons to DreamFusion (Poole et al. 2022), a text-to-3D generation model, and Instruct-NeRF2NeRF (Haque et al. 2023), a NeRF to NeRF translation method using InstructPix2Pix. For DreamFusion, we concatenate additional texts that describe a desired facial expression.

| | Visual Fidelity \uparrow | Text Reflectivity \uparrow | Structural Reflectivity \uparrow |
|--------------------|----------------------------|------------------------------|------------------------------------|
| DreamFusion | 2.11 | 2.68 | 2.88 |
| Instruct-NeRF2NeRF | 3.31 | 3.82 | 3.23 |
| Text2Control3D | 4.92 (+1.61) | 4.55 (+0.73) | 4.87 (+1.64) |

Table 1: User study results. **Best results** are highlighted in bold, and *difference to the second best* is italicized.

| | DreamFusion | Instruct-NeRF2NeRF | Text2Control3D |
|------------------------|-------------|--------------------|----------------|
| R-Precision \uparrow | 65.2 | 56.5 | 69.5 |

Table 2: Evaluating R-Precision using CLIP ViT-L/14. All images are rendered from novel camera views.

Results and Discussion

Qualitative Results We report the qualitative results of our method in Fig. 1 and Fig. 4. The generated 3D avatars faithfully reflects the semantics of the text descriptions, facial expression and the coarse shape of the face in the source monocular video. In addition, despite that contour of the source face remains in the avatars, their unique geometries imply that ControlNet can flexibly handle the depth map conditions to generate images with novel shapes while preserving the viewpoint-aware information implicitly encoded in depth conditions.

Comparison to Baselines The following qualitative comparisons are reported in Fig. 5. As can be seen, the 3D avatars generated from our method shows the highest fidelity and controllability of facial expressions. Since there is no ground truth images to measure PSNR (Mildenhall et al. 2020) or 3D shape to measure Chamfer Distance (Park et al. 2019), we heavily rely on human evaluations for comparisons. Specifically, we asked evaluators to score the quality of results in three criteria: visual fidelity in terms of the overall shape, texture, and color of the faces, text reflectivity in terms of how well the generated avatar is faithful to semantics of the text conditions, and structural reflectivity in terms of how well the generated avatar is faithful to facial expression conditions. We report the average of the responses in Table. 1. As can be seen, results from our methods were preferred by those from baselines in all criteria.

Following prior text-to-3D generation works (Poole et al. 2022), we also computed R-Precision in CLIP ViT-L/14 latent space. Specifically, R-precision measures the percentage of correct retrieval of text that generated the 3D avatar among a set of incorrect texts given the image rendering of the 3D avatar. Our method showed reasonable performance compared to the baselines as reported in Table. 2.

DreamFusion yielded the lowest scores on all user study criteria, inferring lower visual quality than other methods. Occasionally, the 3D shape is also constructed unnaturally as in the third row result. Along with the prevalent Janus problem (Armandpour et al. 2023) observed from SDS-based methods, where frontal appearances are created on side and rear parts of 3D object, these are evidences that SDS with text-to-image diffusion model is not strictly viewpoint-aware, making it unsuitable for sophisticated geometry control for 3D generation.

Instruct-NeRF2NeRF yields reasonable translation results, yet user study responses indicate inferior results than

| | Method | RMSE ↓ | PCK ↑ | CFS ↑ |
|-----|---|-------------|-------------|--------------|
| (a) | $Q = \text{MLP}_Q(h_t^n)$ $K, V = \text{MLP}_{K,V}(h_t^n)$ | 53.2 | 78.4 | 0.682 |
| (b) | $Q = \text{MLP}_Q(\hat{h}_t^n)$ $K, V = \text{MLP}_{K,V}(\hat{h}_t^n)$ | 72.3 | 60.7 | 0.710 |
| (c) | $Q = \text{MLP}_Q(\hat{h}_t^n)$ $K, V = \text{MLP}_{K,V}(h_t^n)$ | 53.2 | 78.4 | 0.684 |
| (d) | $Q = \text{MLP}_Q(\hat{h}_t^n)$ $K, V = \text{MLP}_{K,V}(\hat{h}_t^n)$ | 39.5 | 84.2 | 0.738 |

Table 3: Ablation study on the controllability of facial expression and consistency of appearance over viewpoints.

our method. In addition, translation was not successful in case of the first row result, where hair is not completely removed to translate the source head into bald.

Ablations Table 3 and Fig. 6 show ablation on cross-frame attention and low-pass filtering of Gaussian latents to study their impacts on viewpoint-agnostic texture problem, controllability on facial expressions and appearance across viewpoint-aware images. For facial expression controllability we measure Root Mean Squared Error (RMSE) and Percentage of Correct Key-points (PCK) (Li et al. 2020) between the face key-points of the source and those from the generated avatars, all of which are extracted from images rendered from novel camera views. Consistency in appearance are measured with Cosine Face Similarity (CFS) between avatar images rendered from novel views and an image rendered from a reference view using the off-the-shelf face recognition model¹.

We ablate four major modifications of U-Net in ControlNet: (a) vanilla self-attention, (b) low-pass filtering of Gaussian latent with self-attention, (c) cross-attention of low-pass filtered Gaussian latent features to full-frequency feature that goes through reverse diffusion process in parallel, i.e. Eq. (10) and Eq. (11), and (d) cross-attention of features denoised from low-pass filtered Gaussian latent to reference image with scheduled noise, which is the method we suggest. First column in Fig. 6 are correspondingly generated viewpoint-aware images, and the rest of the columns are images of reconstructed avatars rendered from novel views.

Without low-pass filtering (a) creates viewpoint-agnostic textures that create unwanted artifacts in 3D avatar. However, (b) yields over-smoothed result without cross-attention of low-pass filtered features to full-frequency features. Without cross-attention to a reference image as in (a), (b) and (c), viewpoint-aware images are not coherent in appearance and facial identity, which forces the NeRF model to overfit to varying appearances via view-dependence of the MLP network. Also, inconsistent facial expressions in viewpoint-aware images in (a), (b), and (c) induce NeRF to reconstruct an under-controlled shape. For example in Fig. 6-(a-c), mouths are observed to be closed from the upper view, but are in fact slightly opened when observed from lower views.

¹<https://github.com/ronghuaiyang/arcface-pytorch>

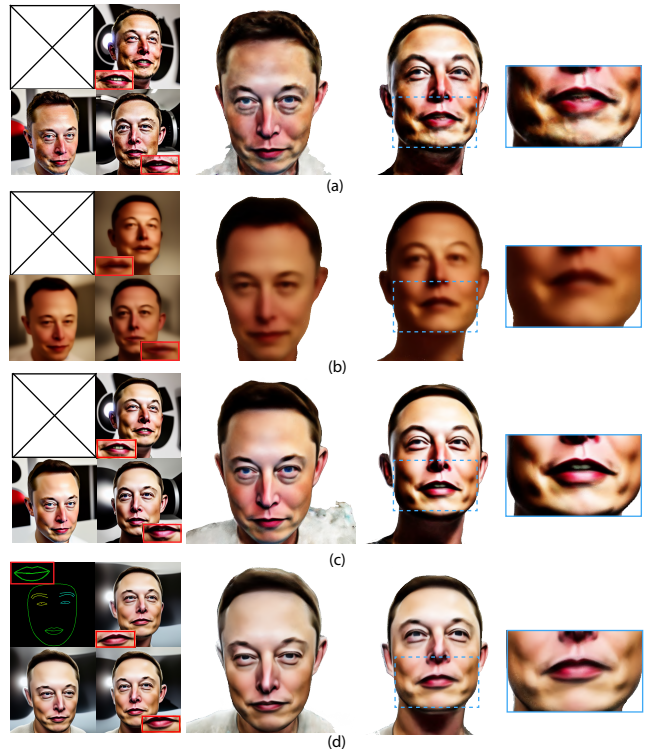


Figure 6: Ablation results. Each row corresponds to modifications in Table. 3. First column shows the viewpoint-aware images and facial key-points if used.

Limitation

One limitation of our method is that key-point conditional ControlNet constructs the controllability bottleneck of our method. For instance, ControlNet often fails to generate reference images with facial expressions that are relatively less common in in-the-wild training images such as closed, winked, frowning eyes. Thus, improvements in controllability of ControlNet via future research can bring parallel improvements to our pipeline in terms of the scope of facial expressions for controlled avatar generation.

Conclusion

We have presented Text2Control3D, the first work to address a controllable text-to-3D avatar generation using text-to-image diffusion model from the best of our knowledge. Our work makes three major contributions: cross-frame attention for viewpoint-aware image generation with controlled facial expression and appearance, low-pass filtering Gaussian latent that ameliorates texture-sticking problem in conditional text-to-image generation, and employing deformable NeRF to reconstruct a 3D avatar using viewpoint-aware yet geometrically inconsistent images. Text2Control3D outperformed the baselines in user-study and quantitative comparisons.

References

An, S.; Xu, H.; Shi, Y.; Song, G.; Ogras, U. Y.; and Luo, L. 2023. PanoHead: Geometry-Aware 3D Full-Head Synthesis

in 360deg. In *Proceedings of the IEEE/CVF Conference on Computer Vision and Pattern Recognition*, 20950–20959.

Anciukevičius, T.; Xu, Z.; Fisher, M.; Henderson, P.; Bilen, H.; Mitra, N. J.; and Guerrero, P. 2023. Renderdiffusion: Image diffusion for 3d reconstruction, inpainting and generation. In *Proceedings of the IEEE/CVF Conference on Computer Vision and Pattern Recognition*, 12608–12618.

Armandpour, M.; Zheng, H.; Sadeghian, A.; Sadeghian, A.; and Zhou, M. 2023. Re-imagine the Negative Prompt Algorithm: Transform 2D Diffusion into 3D, alleviate Janus problem and Beyond. *arXiv preprint arXiv:2304.04968*.

Brigham, E. O. 1988. *The fast Fourier transform and its applications*. Prentice-Hall, Inc.

Chan, E. R.; Lin, C. Z.; Chan, M. A.; Nagano, K.; Pan, B.; De Mello, S.; Gallo, O.; Guibas, L. J.; Tremblay, J.; Khamis, S.; et al. 2022. Efficient geometry-aware 3D generative adversarial networks. In *Proceedings of the IEEE/CVF Conference on Computer Vision and Pattern Recognition*, 16123–16133.

Chan, E. R.; Monteiro, M.; Kellnhofer, P.; Wu, J.; and Wetzstein, G. 2021. pi-gan: Periodic implicit generative adversarial networks for 3d-aware image synthesis. In *Proceedings of the IEEE/CVF conference on computer vision and pattern recognition*, 5799–5809.

Chen, R.; Chen, Y.; Jiao, N.; and Jia, K. 2023. Fantasia3d: Disentangling geometry and appearance for high-quality text-to-3d content creation. *arXiv preprint arXiv:2303.13873*.

Haque, A.; Tancik, M.; Efros, A.; Holynski, A.; and Kanazawa, A. 2023. Instruct-NeRF2NeRF: Editing 3D Scenes with Instructions. In *Proceedings of the IEEE/CVF International Conference on Computer Vision*.

Ho, J.; Jain, A.; and Abbeel, P. 2020. Denoising diffusion probabilistic models. *Advances in neural information processing systems*, 33: 6840–6851.

Karras, T.; Aittala, M.; Laine, S.; Härkönen, E.; Hellsten, J.; Lehtinen, J.; and Aila, T. 2021. Alias-Free Generative Adversarial Networks. In *Proc. NeurIPS*.

Kim, M.; Seo, S.; and Han, B. 2022. InfoNeRF: Ray Entropy Minimization for Few-Shot Neural Volume Rendering. In *Proceedings of the IEEE/CVF Conference on Computer Vision and Pattern Recognition (CVPR)*, 12912–12921.

Li, S.; Ke, L.; Pratama, K.; Tai, Y.-W.; Tang, C.-K.; and Cheng, K.-T. 2020. Cascaded deep monocular 3d human pose estimation with evolutionary training data. In *Proceedings of the IEEE/CVF conference on computer vision and pattern recognition*, 6173–6183.

Li, Y.; Liu, H.; Wu, Q.; Mu, F.; Yang, J.; Gao, J.; Li, C.; and Lee, Y. J. 2023. GLIGEN: Open-Set Grounded Text-to-Image Generation. *CVPR*.

Lin, C.-H.; Gao, J.; Tang, L.; Takikawa, T.; Zeng, X.; Huang, X.; Kreis, K.; Fidler, S.; Liu, M.-Y.; and Lin, T.-Y. 2023. Magic3D: High-Resolution Text-to-3D Content Creation. In *Proceedings of the IEEE/CVF Conference on Computer Vision and Pattern Recognition (CVPR)*, 300–309.

Liu, M.; Xu, C.; Jin, H.; Chen, L.; Xu, Z.; Su, H.; et al. 2023a. One-2-3-45: Any Single Image to 3D Mesh in 45 Seconds without Per-Shape Optimization. *arXiv preprint arXiv:2306.16928*.

Liu, R.; Wu, R.; Van Hoorick, B.; Tokmakov, P.; Zakharov, S.; and Vondrick, C. 2023b. Zero-1-to-3: Zero-shot one image to 3d object. *arXiv preprint arXiv:2303.11328*.

Luo, S.; and Hu, W. 2021. Diffusion probabilistic models for 3d point cloud generation. In *Proceedings of the IEEE/CVF Conference on Computer Vision and Pattern Recognition*, 2837–2845.

Mildenhall, B.; Srinivasan, P. P.; Tancik, M.; Barron, J. T.; Ramamoorthi, R.; and Ng, R. 2020. NeRF: Representing Scenes as Neural Radiance Fields for View Synthesis. In *ECCV*.

Park, J. J.; Florence, P.; Straub, J.; Newcombe, R.; and Lovegrove, S. 2019. Deepsdf: Learning continuous signed distance functions for shape representation. In *Proceedings of the IEEE/CVF conference on computer vision and pattern recognition*, 165–174.

Park, K.; Sinha, U.; Barron, J. T.; Bouaziz, S.; Goldman, D. B.; Seitz, S. M.; and Martin-Brualla, R. 2021a. Nerfies: Deformable neural radiance fields. In *Proceedings of the IEEE/CVF International Conference on Computer Vision*, 5865–5874.

Park, K.; Sinha, U.; Hedman, P.; Barron, J. T.; Bouaziz, S.; Goldman, D. B.; Martin-Brualla, R.; and Seitz, S. M. 2021b. HyperNeRF: a higher-dimensional representation for topologically varying neural radiance fields. *ACM Transactions on Graphics (TOG)*, 40(6): 1–12.

Poole, B.; Jain, A.; Barron, J. T.; and Mildenhall, B. 2022. DreamFusion: Text-to-3D using 2D Diffusion. *arXiv*.

Pumarola, A.; Corona, E.; Pons-Moll, G.; and Moreno-Noguer, F. 2021. D-nerf: Neural radiance fields for dynamic scenes. In *Proceedings of the IEEE/CVF Conference on Computer Vision and Pattern Recognition*, 10318–10327.

Ramesh, A.; Dhariwal, P.; Nichol, A.; Chu, C.; and Chen, M. 2022. Hierarchical text-conditional image generation with clip latents. *arXiv preprint arXiv:2204.06125*.

Ramesh, A.; Pavlov, M.; Goh, G.; Gray, S.; Voss, C.; Radford, A.; Chen, M.; and Sutskever, I. 2021. Zero-shot text-to-image generation. In *International Conference on Machine Learning*, 8821–8831. PMLR.

Rombach, R.; Blattmann, A.; Lorenz, D.; Esser, P.; and Ommer, B. 2021. High-Resolution Image Synthesis with Latent Diffusion Models. *arXiv:2112.10752*.

Saharia, C.; Chan, W.; Saxena, S.; Li, L.; Whang, J.; Denton, E. L.; Ghasemipour, K.; Gontijo Lopes, R.; Karagol Ayan, B.; Salimans, T.; et al. 2022. Photorealistic text-to-image diffusion models with deep language understanding. *Advances in Neural Information Processing Systems*, 35: 36479–36494.

Shannon, C. E. 1948. A mathematical theory of communication. *The Bell system technical journal*, 27(3): 379–423.

Shue, J. R.; Chan, E. R.; Po, R.; Ankner, Z.; Wu, J.; and Wetzstein, G. 2023. 3d neural field generation using triplane

diffusion. In *Proceedings of the IEEE/CVF Conference on Computer Vision and Pattern Recognition*, 20875–20886.

Song, J.; Meng, C.; and Ermon, S. 2020. Denoising Diffusion Implicit Models. In *International Conference on Learning Representations*.

Zhang, L.; and Agrawala, M. 2023. Adding Conditional Control to Text-to-Image Diffusion Models. arXiv:2302.05543.